



Intravitreal injection of new adeno-associated viral vector: Enhancing retinoschisin 1 gene transduction in a mouse model of X-linked retinoschisis

Yan Sun^{a,b}, Dan Xiao^a, Zhuang Li^a, Dan Xu^b, Donglei Zhang^b, Yuanlong An^b, Jinyue Xue^b, Yue Ren^a, Shu Liu^a, Di Wang^a, Jun Li^{a,**}, Zhuoshi Wang^{a,b,***}, Jijing Pang^{a,b,*}

^a Shenyang He Eye Specialist Hospital, Shenyang, China

^b He University, Shenyang, China

ABSTRACT

Adeno-associated virus (AAV) vectors have been widely used in therapy to treat hereditary retinal diseases. But its transduction efficiency by intravitreal injection still needs to be improved. In this study, we investigated the transduction efficiency of AAV-DJ (K137R)-GFP in different retinal cells of normal mice, as well as the therapy effect of AAV-DJ (K137R)-Rs1 on retinal function and structure in Rs1-KO mice. The intravitreal injection of AAV-DJ (K137R)-GFP demonstrated that this vector transduced cells in all layers of the retina, including the inner nuclear layer and photoreceptor layer. The intravitreal injection of AAV-DJ (K137R)-Rs1 found that 3 months post-injection of this vector improved retinal function and structure in Rs1-KO mice. Our conclusion is that AAV-DJ (K137R) vector can efficiently and safely penetrate the inner limiting membrane and transduce different layers of retinal cells in the long term, as well as being able to continuously and efficiently express target therapeutic proteins, making it a candidate therapeutic vector for X-linked retinoschisis (XLRS).

1. Introduction

X-linked retinoschisis (XLRS) causes macular degeneration in males and is characterized by structural changes in the retina [1,2]. Evidence obtained using ocular coherence tomography (OCT) shows that intraretinal splitting can involve all retinal layers [3,4]. XLRS phenotypes result from the loss of retinoschisin function [5–9]. Thus, basic countermeasures for treating XLRS patients and Rs1-deficient mice (Rs1-KO) is to replace the deleted retinoschisin protein via gene therapy.

AAV vectors have become among the most promising delivery systems for the treatment of hereditary retinal diseases [10–12]. They are also suitable for use in the treatment of retinoschisis. Studies have shown that the target gene can be effectively delivered to the retinal pigment epithelium and photoreceptor layer through the subretinal injection of the adeno-associated viral vector. However, subretinal injection is relatively invasive. After intravitreal injection, although the damage caused by the carrier is reduced, it remains difficult for the carrier to penetrate the inner-boundary membrane and reach the inner retina [13–15]. Currently, the only two adeno-associated viral vectors for intravitreal injection used to treat eye disease have failed to achieve the

expected therapeutic effects [15,16]. The search for a new vector of AAV that can be used to safely and effectively treat intraocular retinal diseases through intravitreal injection constitutes a reliable research and development direction.

AAV-DJ can be transduced into retinal cells via a simple and easy intravitreal injection [17], but its transduction efficiency still needs to be improved. A promising approach to achieving higher transduction efficiency is to rationally design mutations of tyrosine residues exposed on the capsid surface. Currently, the main surface design mutants of the AAV-DJ capsid is K137R. Its use leads to better transduction efficiency in both in vitro experiments and in liver tissues than other vectors. However, the transduction efficiency of K137R vectors in other tissues remains unknown. Thus, this study aims to confirm the transduction efficiency of the AAV-DJ (K137R) mutant by testing its transduction mode in the retina via intravitreal injection, and testing its therapeutic effect on the XLRS diseases. This study is the first to use a tyrosine-modified AAV-DJ vector for ophthalmic gene therapy. This research lays the foundation for the development of new AAV-DJ mutants and the long-term safe and effective treatment of inherited retinal diseases.

* Corresponding author. Shenyang He Eye Specialist Hospital, Shenyang, China.

** Corresponding author. Shenyang He Eye Specialist Hospital, Shenyang, China.

*** Corresponding author. He University, Shenyang, China.

E-mail addresses: lijun01@hsyk.com.cn (J. Li), dr.wangzs@foxmail.com (Z. Wang), jjpangoph@hotmail.com (J. Pang).

2. Materials and methods

2.1. Animals

C57 BL/6J mice and Rs1-KO mice were obtained from the Liaoning Changsheng Biotechnology Co., Ltd. and bred at the He University. Unless otherwise specified, all mice were housed in the He University Animal Center Animal Care Services Facilities, following a 12-h light/12-h dark cycle with less than 15 ft-c environmental illumination. Rs1-KO mice used Rs1-201 as the target gene sequence for the gene knockout. The natural history of the Rs1-KO model has been documented and validated. The phenotype was consistent with the clinical phenotype of retinoschisis. Seventy C57 BL/6J mice (male = 42, female = 28) and forty-one Rs1-KO mice (male = 24, female = 17) were used in this study. Rs1-KO mouse models were homozygous X mutant mice, and mouse phenotypes were included by uniform inclusion criteria, and there was no difference in genotype and phenotype involved between different genders. All experiments were approved by He university Committee for Laboratory Animal Welfare and Ethical (IACUC Issue No.2022021501, Approval Date:20220506) and conducted in accordance with the National Institutes of Health guide for the care and use of Laboratory animals (NIH Publications No. 8023, revised 1978).

2.2. Production of vectors

The AAV8-GFP, AAV-DJ-GFP, AAV-DJ(K137R)-GFP, AAV-DJ-Rs1, and AAV-DJ(K137R)-Rs1 vectors were driven by the CBA promoter. These vectors were prepared using the plasmid cotransfection method. The AAV-GFP and its auxiliary plasmids were cotransfected into 293T cells using the calcium carbonate method, and the virus was collected 72 h after transfection. The cells were centrifuged at 4000 rpm for 20 min, the supernatant was discarded, and the cell precipitates were resuspended with 2 ml of PBS and stored at -20°C . Then, the virus was purified using cesium chloride density gradient centrifugation and the venom was concentrated using a Millipore column. Viral titers were determined using a quantitative polymerase chain reaction, and the final preparation was diluted and subpackaged with phosphate-buffered saline (PBS) before being stored at -80°C .

2.3. Intraocular administration of vector

We administered 0.5 % tropicamide phenylephrine eye drops to achieve quick mydriasis 30 min prior to anesthesia. We anesthetized the mice with a mixture of Telazol (50 mg/kg) and xylazine (5 mg/kg bodyweight). Then, 1 μL of target vectors (containing $1\text{E}10$ genome vector particles) was administered to the intravitreal space of mice, including AAV8-GFP (N = 9), AAV-DJ-GFP (N = 36), AAV-DJ(K137R)-GFP (N = 16), AAV-DJ-Rs1 (N = 19), AAV-DJ(K137R)-Rs1 (N = 15) and PBS (vehicle, N = 9 (C57 BL/6J), N = 7 (Rs1-KO)). After all injections, 1 % atropine eye drops and dexamethasone ophthalmic ointment were administered.

2.4. Fundus photography

Fundus fluorescence imaging was performed using a digital fundus camera (OPTO-RIS, Retinal Imaging System, OptoProbe, UK) at 14/21/28/35 days and 3 months, 6 months, 12 months post-injection. This followed the anaesthetization of animals and dilation of their pupils as mentioned above. In order to further investigate the duration of AAV-DJ (K137R) and AAV-DJ expression, we chose to continue feeding several mice with fundus fluorescence, and observed the changes of fundus fluorescence at 3 months, 6 months and 12 months after the injections.

2.5. Electroretinography

Mice were permitted to adapt to the dark over a period of 24 h, after

which they were given an anaesthetization and their eyes were dilated. The mice were then placed onto a heated platform (37°C). Two gold-wire electrodes were placed onto the corneal surface of eyes and connected to a goldwire in the subcutaneous of overhead. A pin electrode in the tail served as the ground. We performed the ERG procedure using an OPTO - III visual electrophysiology instrument (Optoprobe, UK), as described previously. The maximum mixing reaction amplification factor of the stimulus light parameters was 4K (low-frequency, 75 Hz; high-frequency, 300 Hz; flash brightness, white light 600s/m²; flash stimulus, 5 ms; flash intensity, 3.0 cd s/m²; and stimulus interval, 15s).

2.6. Optical coherence tomography

Each layer of retinal thickness in mice was examined using a retinal imaging system via optical coherence tomography (OCT, OPTOPROBE, UK). Mice were anesthetized and their eyes were dilated using 0.5 % tropicamide eye drops. Then, images were captured and retinal thickness was calculated using an analysis software (Version 2.0, OptoProbe Research Ltd. The two measurements were averaged to give a single value for each retina. The corresponding neural retina thickness for treated and untreated eyes was compared at 1000 μm from the optic nerve in the nasal and temporal retina by measuring the average distance from the vitreal face of the ganglion cell layer to the apical face of the retinal pigment epithelium. The identity of the samples was masked at the time of measurement.

2.7. Wholemounts and cryosections

Thirty-five days post-injection, the mice were euthanized in a humane manner. The eyes were then removed and fixed using a 4 % paraformaldehyde solution in phosphate-buffered saline for 1 h. Subsequently, the cornea and lens were removed. To create flat mounts, the entire retina was carefully dissected from the eyecup and radial cuts were made from the edges to the equator of the retina. For cryosections, the eyecups were washed in phosphate-buffered saline and then immersed in a 30 % sucrose solution in the same buffer overnight. The eyes were subsequently embedded in optimal cutting temperature embedding compound (Tissue-Tek, SAKURA, Japan) and oriented in order to obtain 8 μm thick transverse retinal sections.

2.8. Immunohistochemistry

Tissue sections were incubated with 0.5 % Triton X-100 for 15 min, and then washed three times with phosphate-buffered saline for 5 min each. The sections were stained using RS1 Polyclonal antibody (Proteintech) and a secondary antibody conjugated to CoraLite®488-Conjugated AffiniPure Goat Anti-Rabbit IgG(H + L) (Proteintech). Nuclei were stained with DAPI before being finally sealed with an anti-fluorescence quencher. Retinal flat mounts and sections were examined using a CLIPSE Ci/NiU fluorescence microscope (Nikon, Japan).

2.9. Statistical analysis

The GFP staining intensity in flat mounts was quantified from fluorescence microscopic images using Image J software (National Institutes of Health) in order to determine the fluorescence intensity in pixels per unit area. ERG amplitude and OCT results were evaluated by calculating the ratio of the treated eye to the untreated eye (T/UT) in each mouse and averaging these values for each vector. Outliers in the T/UT values for each vector were removed using the ROUT method before performing statistical analysis. All data were expressed as the mean \pm S.E.M and differences between groups were evaluated using GraphPad Prism software (GraphPad Prism 9; GraphPad, La Jolla, CA), with one-way ANOVA followed by Dunnett's post-test for group comparison. A p value < 0.05 was considered to be statistically significant and represented as follows; *: p < 0.05 , **: p < 0.01 , ***: p < 0.001 , ****: p $<$

0.0001.

3. Results

3.1. The transfection effect of AAV-DJ (K137R)-GFP, AAV-DJ-GFP and AAV8-GFP vector

We first observed the time course of enhanced expression of green fluorescent protein (GFP) in the retina of mice after the intravitreal injection of AAV. Images taken at 14d\21d\28d\35d\3 M\6 M\12 M post-injection into the vitreous cavity clearly showed the fluorescence expression in the retina, with the optic disc as the focal point. Among them, AAV-DJ-GFP and AAV-DJ (K137R)-GFP vectors showed GFP fluorescence expression on day 14 after injection, the fluorescence intensity reached its peak 35 days after injection, and the GFP fluorescence was still detected at 12 months after fluorescence (Fig. 1A-R). However, the fluorescence expression time and intensity of AAV8-GFP were not as expected. Meanwhile, we found that, compared to AAV-DJ-GFP, AAV-DJ (K137R)-GFP vectors can maintain fluorescence expression for a longer period of time.

From the perspective of fluorescence expression intensity and area, the fluorescence expression of the three vectors was mainly distributed along the optic disc and blood vessels. After 35 days, it began to diffuse along the optic nerve fibers towards the periphery, and the fluorescence area gradually expanded, while the fluorescence intensity gradually weakened over time. By comparing the fluorescence intensity from 14 days to 12 months after surgery, it was found that the maximum intensity and area of fluorescence expression of AAV-DJ (K137R)-GFP were significantly greater than those of AAV8 and AAV-DJ-GFP vectors (Fig. 2A and B). At the same time, we found that compared to AAV-DJ-GFP, AAV-DJ(K137R)-GFP had a significantly higher GFP protein expression in the retina from 35 days after injection compared to AAV-DJ-GFP. At the same time, it still maintained high fluorescent protein expression and large transfection area 3 months after injection, and persisted in doing so for more than 12 months (Fig. 2C). The OCT examination also did not reveal any structural retinal abnormalities

(Fig. 2G).

The expression of GFP in the retina was observed in the entirety of mounted retina after 35 days of intravitreal injection. GFP expression in the retina injected with AAV8 was limited to the optic disc (Fig. 3A). In contrast, injection of AAV-DJ-GFP and AAV-DJ (K137R)-GFP showed the accumulation of GFP signals in specific areas, such as around the blood vessels covering the Müller glial processes and around the optic disc (Fig. 3B, C and 3D). Immunohistochemical analyses revealed GFP fluorescence expression in nerve fiber cells, horizontal cells, and Müller cells for AAV-DJ-GFP and AAV-DJ(K137R)-GFP (Fig. 3F and G).

3.2. The transfection effect of AAV-DJ (K137R) -Rs1

The a-wave and b-wave in the untreated eye were disproportionately reduced compared with the WT. Conversely, the fellow eye treated with AAV-DJ(K137R)-Rs1 had a substantially larger a-wave amplitude and b-wave amplitude. In OCT images, the untreated eye possessed widely distributed, large cavities. Their presence increased opl-inl of retinal thickness compared with WT, but cavities were reduced from the fellow eye treated using AAV-DJ(K137R)-Rs1. This phenomenon was observed from the HE staining of images of paraffin sections. Both WT- and Rs1-KO-treated mice showed green immunofluorescence in their retinas, with none observed in the untreated retinas of Rs1-KO mice. Comparing the ability of the AAV-DJ(K137R)-Rs1 and AAV-DJ-Rs1-treated eyes to improve retinal function and structure, the AAV-DJ(K137R)-Rs1-treated eye was more effective in increasing b-wave amplitude and shrinking cystic cavity (Fig. 4).

The b-wave/a-wave amplitude ratio results showed that, compared to the vehicle group, the ratio of treated eyes to untreated eyes (T/UT) for the AAV-DJ (K137R)-Rs1 group improved by 25 % ($p < 0.05$; Fig. 5A and B). However, the ratio of treated to untreated eyes (T/UT) for the AAV-DJ-Rs1 group showed no statistically significant difference compared to the vehicle group. By comparing the opl-inl thickness ratio (T/UT) between the treated and untreated eyes in the vehicle group, AAV-DJ-Rs1 group, and AAV-DJ (K137R)-Rs1 group, we found that the opl-inl thickness value in the AAV-DJ (K137R)-Rs1 group was

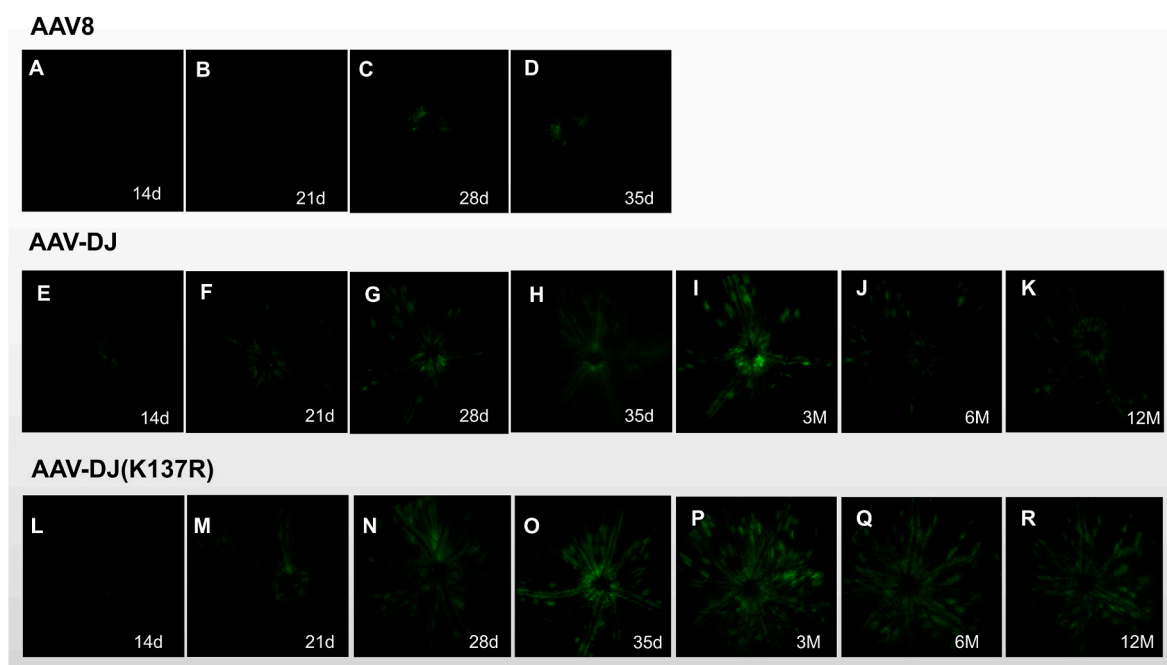


Fig. 1. Time course of GFP expression in the retina following AAV intravitreal injection. Representative fundus photographs show GFP expression in different live mice from 14 days through 12 M after the AAV injection. (A), (B), (C), (D): AAV8-GFP; (E), (F), (G), (H), (I),(J),(K): AAV-DJ-GFP; (L), (M), (N), (O),(P),(Q),(R): AAV-DJ (K137R)-GFP; GFP stands for green fluorescent protein. Fundus photography field is 50°, and approximately 25 % of the central retinal extent is covered. (For interpretation of the references to color in this figure legend, the reader is referred to the Web version of this article.)

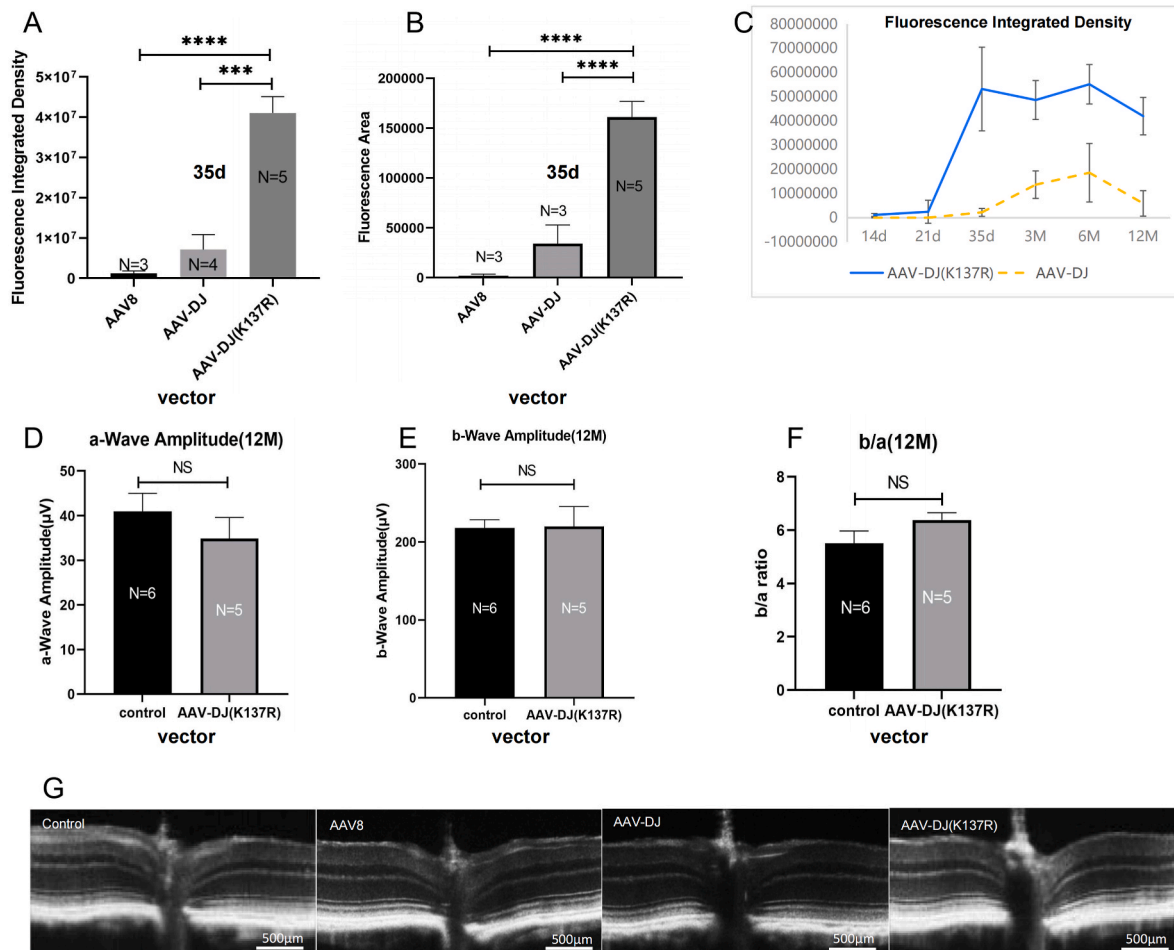


Fig. 2. Intensity and areal analysis of GFP fluorescence expression and effect on visual function after injection of three vectors. (A): Comparison of GFP fluorescence intensity in retinal fundus images between three vectors. (B): Comparison of GFP fluorescence area in retinal fundus images between three vectors. (C): Comparison of GFP intensity in retinal fundus images at different time points after vitreous cavity injection of three vectors. (D): Average a-wave amplitude for 12 months. (E): Average b-wave amplitude for 12 months; (F): Average b-wave/a-wave amplitude for 12 months. (G): Representative OCT images of vectors. All pictures were taken with the same exposure time in order to evaluate GFP intensity using Image J. Scale bars, 500 μm in G. Error bars represent the standard error of the mean. NS indicates not significant. *** $p < 0.001$, analysis of variance.

significantly reduced.

4. Discussion

The physical barrier between the posterior limiting membrane of the vitreous body and the inner limiting membrane of the retina is the primary challenge hindering clinical trials of gene therapy for retinoschisis [3,4]. Choosing the appropriate AAV serotype and modifying the AAV capsid to improve transfection efficiency is a feasible method. K137R mutant based on AAV-DJ vector was a modified vector. A study suggested that AAV-DJ vector could mediate efficient gene expression both in vitro and in vivo [17], and another study indicated that K137R mutation on the basis of AAV8 had significantly higher systemic transduction efficiency, possibly due to decreased ubiquitination of the viral capsid resulting in rapid intracellular trafficking of the virus and improved gene expression [18]. A major barrier that negatively affects AAV-mediated gene expression is the degradation of the viral particles during their intracellular trafficking via the ubiquitination-proteasomal degradation machinery [19]. As a measure to evade phosphorylation and subsequent ubiquitination leading to vector loss. Lysine (K) amino acids as potential cellular kinase or ubiquitination targets, which, when substituted with compatible amino acids, improved AAV2 transduction in vitro and in vivo [20]. So in this study confirmed a gene therapy vector with higher transfection efficiency in the retina by testing the

amino acid K137R point mutation on the surface of AAV-DJ capsid, and attempted to apply this new vector to ophthalmology for the first time. Then, this study evaluated the penetration ability of the new vector in the retina and the expression ability, as well as the therapeutic effect of the gene therapy vector drug on the Rs1-KO mouse model.

In this study, we observed that fundus fluorescence accumulates around the optic disc and blood vessels and determined that it might be suitable for use in gene therapy, whether targeting retinal vascular lesions via anti-angiogenic therapy [21,22] or treating optic disc diseases. At the same time, the modified AAV-DJ (K137R)-GFP can more efficiently pass through the inner limiting membrane and be transduced to outer retinal cells. This means that GFP protein is expressed from the GCL layer to the outer membrane. We believe that the improvement in penetration efficiency and expression efficiency is related to the lysine structure on the surface of the improved AAV capsid in this study. This study confirms that the modified design of the AAV-DJ (K137R)-GFP can mutate the target tyrosine, causing it to be unable to be phosphorylated, thereby targeting the regulation of tyrosine kinase activity, improving AAV penetration, and increasing Rs1 protein expression. Based on these findings, we predict that AAV-DJ (K137R) may be suitable for targeted gene therapy to central fovea or Müller cell lesions [23], as well as the safe treatment of XLRP [12,24]. Due to the pathological changes of these diseases, permanent trauma caused by subretinal injection cannot be tolerated. However, intravitreal injection can maximize the therapeutic

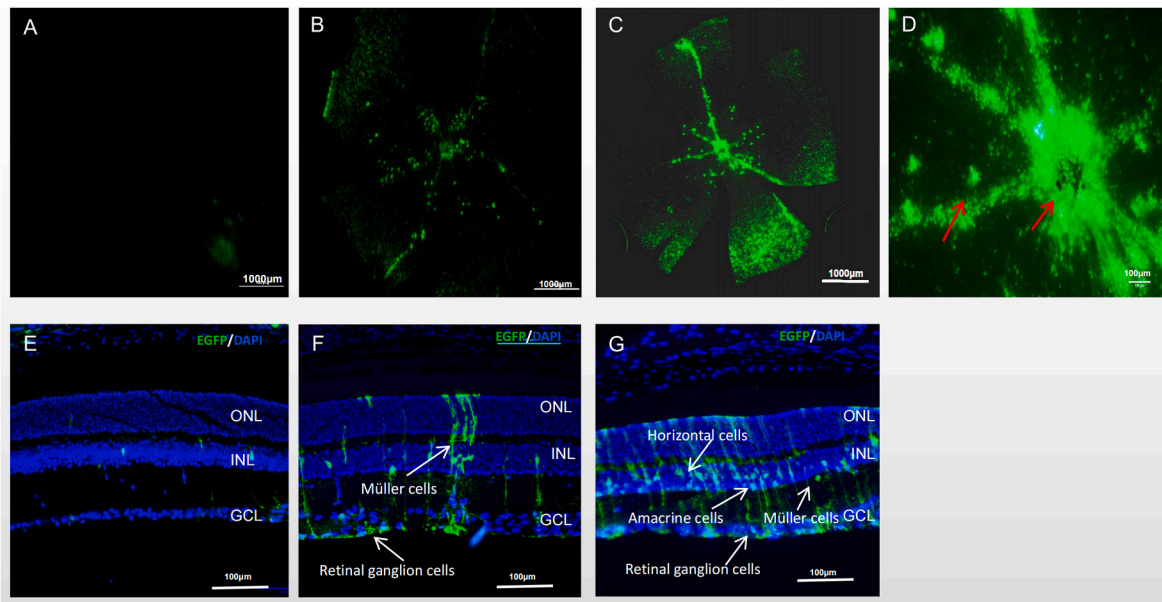


Fig. 3. GFP expression in the murine retina following intravitreal injection of three AAV vectors. The representative confocal images display whole-mount retina (A, B, C and D) and cross sections of retinas (E, F, and G) taken 35 days after intravitreal injection. AAV8-GFP (A and E), AAV-DJ-GFP (B and F), AAV-DJ (K137R)-GFP (C, D and G). The red arrow shows the aggregated area of transduced retinal cells(D). The blue color represents DAPI nuclear counterstain. Scale bars, 1000 μm in A, B and C, and 100 μm in D, E, F and G. (For interpretation of the references to color in this figure legend, the reader is referred to the Web version of this article.)

benefits of specific high-expression AAV-DJ (K137R) vectors.

In addition to focusing on the fluorescence intensity and penetration depth of GFP protein, we also investigated the transduction speed and long-term expression ability of AAV vectors [23,24] as an earlier expression time indicates a higher transduction speed, while longer sustained expression time indicates a more stable expression sequence for the vector after transduction. Most AAV-GFP vectors exhibit observable GFP protein expression starting from 10 to 14 days [15]. Unfortunately, most studies have not observed sustained AAV vector expression over 6 months. This study is the first to explore the long-term sustained expression of the AAV-DJ (K137R)-GFP vector in the retina after intravitreal injection (>12 months). The results showed that the AAV-DJ (K137R)-GFP vector could observe circular low fluorescence around the optic disc 14 days after injection into the vitreous body, reaching the highest fluorescence intensity (peak) at 35 days, and that GFP expression with high fluorescence intensity could still be observed 12 months after injection. In contrast, the fluorescence intensity of GFP proteins carried by AAV2 and AAV8 vectors began to decrease 12 months after intravitreal injection [25,26]. Therefore, we believe that the modified mutation vector possesses unique advantages in terms of transduction speed and sustained expression. As such, its use helps to achieve faster therapeutic effects and more durable and stable functional improvements in clinical applications.

We further investigated the therapeutic effect of AAV-DJ (K137R) carrying RS1 gene on RS1-ko mice. The results showed that in the XLR5 model Rs1-KO mouse experiment, the application of the AAV-DJ (K137R) - RS1 vector through a single intravitreal injection significantly improved the retinal structure, which manifested as a decrease in the opl-inl layer and a reduction in the capsule cavity. The increase in the amplitude ratio of b-wave and a-wave resulted in improved function, which is consistent with other studies [24,25]. We speculate that AAV-DJ (K137R)-RS1 adeno-associated virus vector can transmit homologous RS1 protein to compensate for the missing RS1 protein in RS1-ko mice. This could be seen from the immunofluorescence staining of AAV-DJ (K137R) - GFP and AAV-DJ (K137R) - RS1, which were expressed from the IS layer to the outer membrane after intravitreal injection, and were more strongly expressed on Müller cells. The RS1 protein produced had a certain adhesive effect on retinal cells, thereby

reducing the retinal capsule space. The enhanced intercellular adhesion repaired a portion of the transmission of retinal electrical signals, thereby improving the visual function of RS1-KO mice [17,24,26,27]. These alterations will help the vector to obtain an earlier expression time and stronger transduction efficiency.

Of course, this study had some limitations. We did not conduct RT-qPCR and Western blotting to accurately quantify mRNA and protein expression, and we need to supplement these data in subsequent experiments. Our study did not observe retinal fluorescence expression after 12 months. These data will be supplemented into subsequent studies. The sample size of this study was small, and more samples are needed in subsequent experiments to verify its conclusions. We did not study the membrane penetration of K137R using in vitro experimental methods, but other studies provided an in vitro experimental method to verify the membrane penetration [28]. We will consider this method to further explore the membrane penetration of K137R mutants in our future studies.

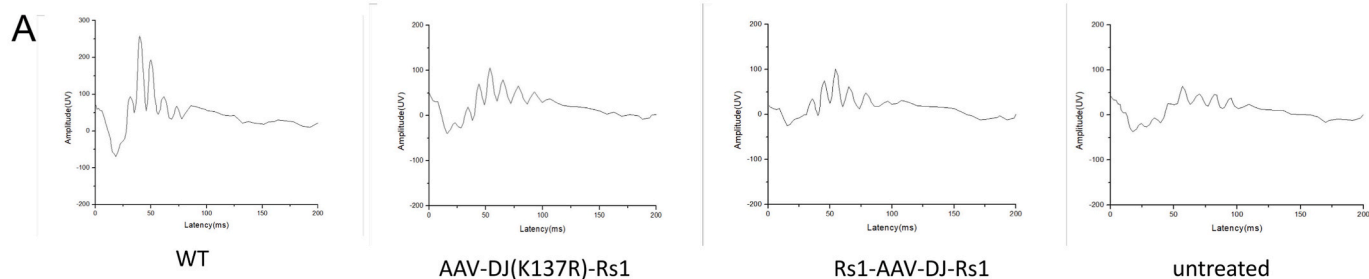
In conclusion, this study is the first to use a tyrosine-modified AAV-DJ vector for ophthalmic gene therapy and observe the long-term gene therapy effect of this vector on retinoschisis. The study demonstrated that the AAV-DJ(K137R) vector modified with tyrosine sites can be transfected into full-layer retinal cells via intravitreal injection and has a larger range of retinal transfection efficiency than traditional unmodified vectors. At the same time, AAV-DJ(K137R) also demonstrates the potential for long-term and efficient expression of specific proteins in the target region, especially in the optic disc and retinal vascular regions. This study did not observe any adverse effects or long-term risks of AAV-DJ(K137R) vector regarding retinal function and structure. Our study provides benefit by offering valuable insights into the behavior of this mutation vectors in retinal cells and aiding in the development of improved protocols and novel ideas for treating X-linked retinoschisis diseases.

CRediT authorship contribution statement

Yan Sun: Writing – review & editing, Writing – original draft, Validation, Project administration, Formal analysis. **Dan Xiao:** Visualization, Validation, Investigation. **Zhuang Li:** Software, Data curation.

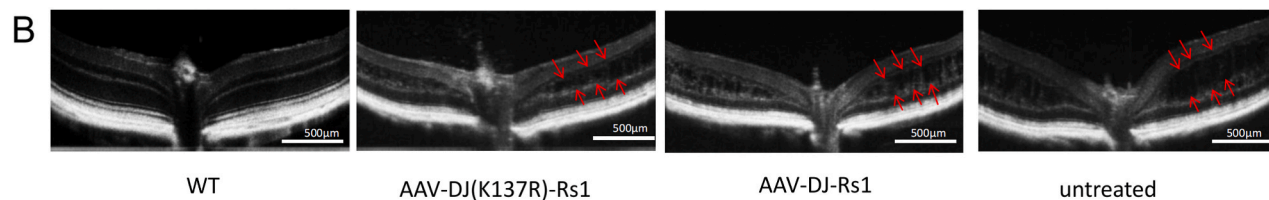
Function

ERG



Structure

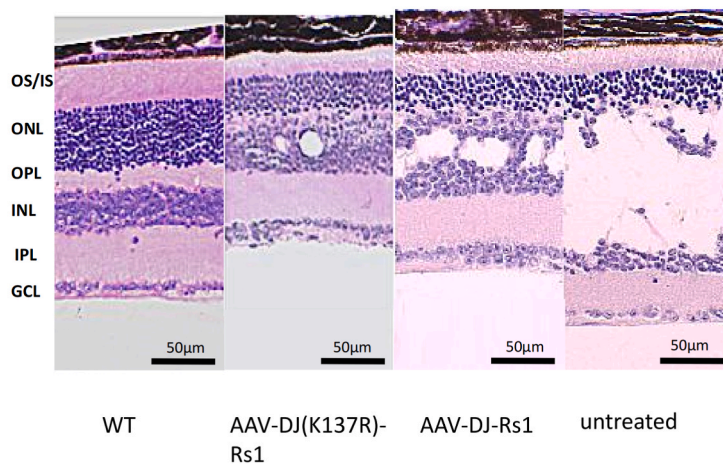
OCT



C

Structure

HE



D

RS1 Protein

IHC

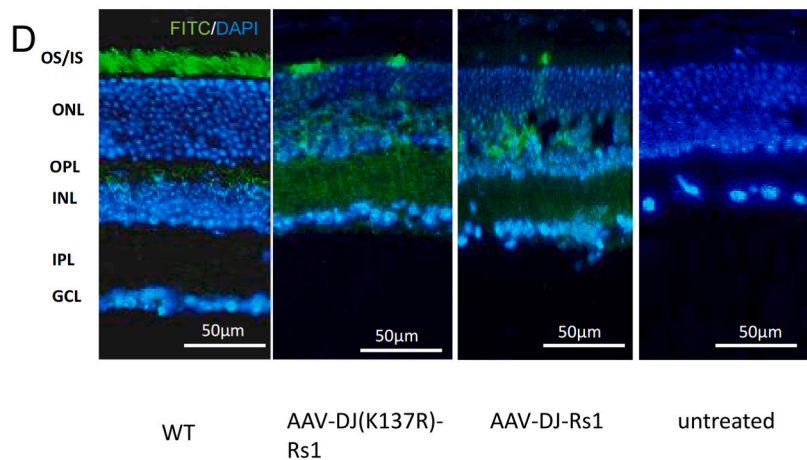


Fig. 4. Improvement of retinal function and structure in Rs1-KO mouse model after 3 months of intravitreal injection of AAV-DJ(K137R)-Rs1 and AAV-DJ-Rs1 vector. ERG, OCT, HE, and IHC were used for evaluation. (A): Representative ERG waveforms. (B): Representative OCT images. (C): HE staining. (D): Immunohistochemistry staining. The red arrow indicates the boundary of the cavity. The untreated eye has large cavities spanning layers proximal to the photoreceptor nuclear layer (ONL). Scale bar, 500µm in B, 50 µm in C and D. (For interpretation of the references to color in this figure legend, the reader is referred to the Web version of this article.)

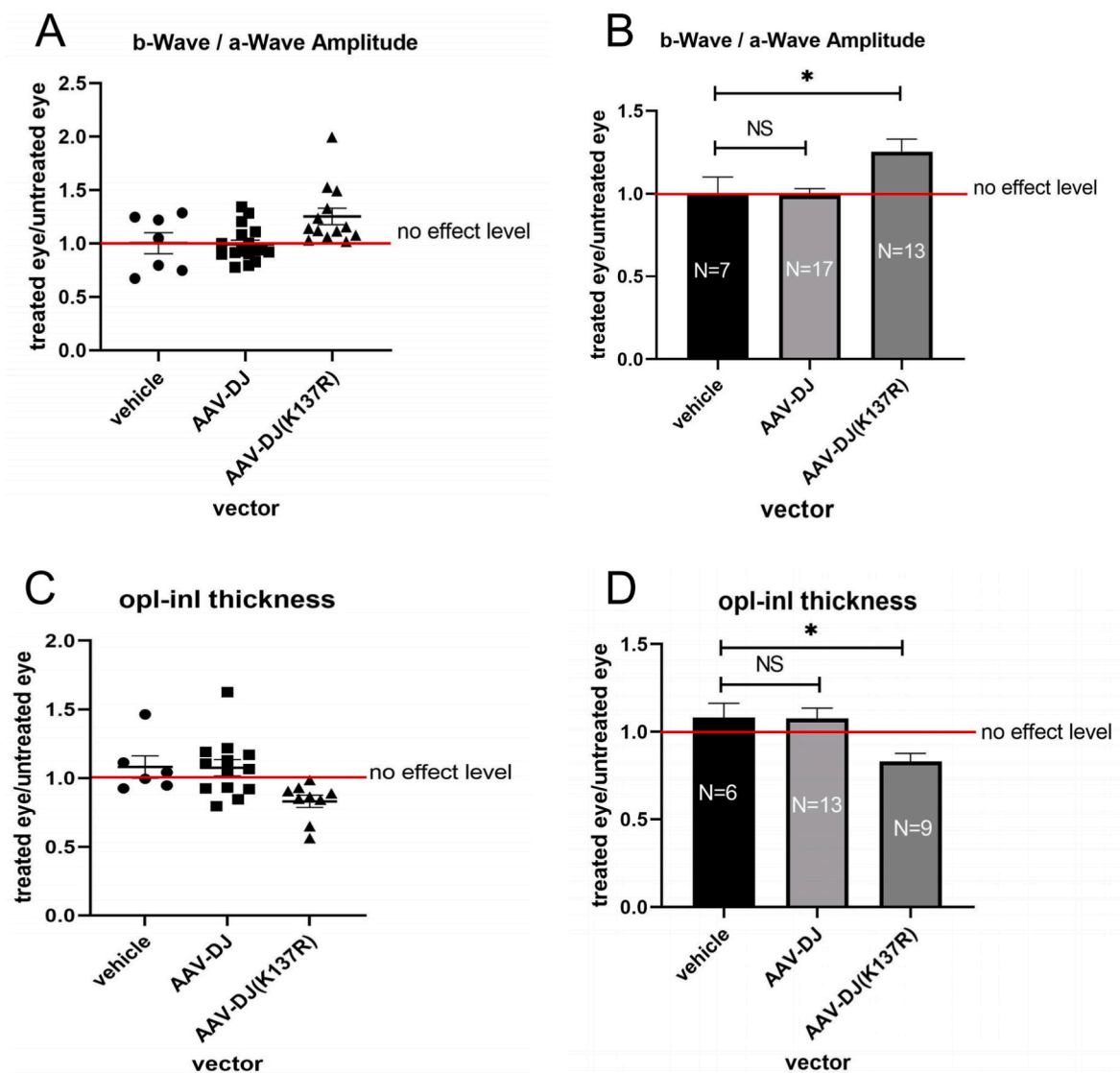


Fig. 5. Statistical analysis of ERG and OCT data after 3 months of treatment with AAV-DJ (K137R)-Rs1. The ratio of the treated eye to the untreated eye (T/UT) is plotted for the b-wave/a-wave amplitude and opl-inl thickness. (A): The scatter plots show the b-wave/a-wave amplitude results from individual mice at each vector. (B): The bar graphs show the averages and SEM of b-wave/a-wave amplitude for each vector. (C): The scatter plots show the opl-inl thickness results from individual mice at each vector. (D): The bar graphs show the averages and SEM of opl-inl thickness for each vector. Asterisks indicate significance of treatment effect compared with vehicle (**** $p < 0.0001$, ** $p < 0.01$, * $p < 0.05$). NS indicates 'not significant'.

Dan Xu: Validation, Data curation. **Donglei Zhang:** Resources, Funding acquisition. **Yuanlong An:** Validation, Resources. **Jinyue Xue:** Validation, Data curation. **Yue Ren:** Visualization, Investigation. **Shu Liu:** Visualization, Investigation. **Di Wang:** Visualization, Investigation. **Jun Li:** Writing – review & editing, Supervision, Conceptualization. **Zhuoshi Wang:** Supervision, Resources, Methodology, Funding acquisition. **Jijiang Pang:** Writing – review & editing, Methodology, Funding acquisition, Conceptualization.

Declaration of competing interest

The authors declare that they have no known competing financial interests or personal relationships that could have appeared to influence the work reported in this paper.

Data availability

Data will be made available on request.

Acknowledgements

The authors sincerely thank all of the all colleagues in the animal laboratory who participated in this study. In addition, the authors would like to thank Liaoning Changsheng Biotechnology Co., Ltd for their technical support and the staff at He University for their assistance. The manuscript was edited by professional English editing service. Finally, this work was supported by the Shenyang Municipal Bureau of Science and Technology Project [No.20-3014-001] and the National Natural Science Foundation of China (81970840).

References

- [1] S.K. Sikkink, S. Biswas, N.R. Parry, P.E. Stanga, D. Trump, X-linked retinoschisis: an update, *J. Med. Genet.* 44 (2007) 225–232, <https://doi.org/10.1136/jmg.2006.047340>.
- [2] A. Tantri, T.R. Vrabec, A. Cu-Unjieng, A. Frost, W.H. Annesley Jr., L.A. Donoso, X-linked retinoschisis: a clinical and molecular genetic review, *Surv. Ophthalmol.* 49 (2004) 214–230, <https://doi.org/10.1016/j.survophthal.2003.12.007>.

- [3] J.L. Prenner, A. Capone Jr., S. Ciaccia, Y. Takada, P.A. Sieving, M.T. Trese, Congenital X-linked retinoschisis classification system, *Retina* 26 (2006) S61–S64, <https://doi.org/10.1097/01.iae.0000244290.09499.c1>.
- [4] Y. Minami, S. Ishiko, Y. Takai, Y. Kato, H. Kagokawa, A. Takamiya, T. Nagaoka, R. Kinouchi, A. Yoshida, Retinal changes in juvenile X linked retinoschisis using three dimensional optical coherence tomography, *Br. J. Ophthalmol.* 89 (2005) 1663–1664, <https://doi.org/10.1136/bjo.2005.075648>.
- [5] L.L. Molday, D. Hicks, C.G. Sauer, B.H. Weber, R.S. Molday, Expression of X-linked retinoschisis protein RS1 in photoreceptor and bipolar cells, *Invest. Ophthalmol. Vis. Sci.* 42 (2001) 816–825.
- [6] Y. Takada, R.N. Fariss, A. Tanikawa, Y. Zeng, D. Carper, R. Bush, P.A. Sieving, A retinal neuronal developmental wave of retinoschisin expression begins in ganglion cells during layer formation, *Invest. Ophthalmol. Vis. Sci.* 45 (2004) 3302–3312, <https://doi.org/10.1167/iovs.04-0156>.
- [7] G. Tolun, C. Vijayasathary, R. Huang, Y. Zeng, Y. Li, A.C. Steven, P.A. Sieving, J. B. Heymann, Paired octamer rings of retinoschisin suggest a junctional model for cell-cell adhesion in the retina, *Proc. Natl. Acad. Sci. U.S.A.* 113 (2016) 5287–5292, <https://doi.org/10.1073/pnas.1519048113>.
- [8] S.N. Reid, C. Yamashita, D.B. Farber, Retinoschisin, a photoreceptor-secreted protein, and its interaction with bipolar and muller cells, *J. Neurosci.* 23 (2003) 6030–6040, <https://doi.org/10.1523/JNEUROSCI.23-14-06030.2003>.
- [9] Functional implications of the spectrum of mutations found in 234 cases with X-linked juvenile retinoschisis. The Retinoschisis Consortium, *Hum. Mol. Genet.* 7 (1998) 1185–1192, <https://doi.org/10.1093/hmg/7.7.1185>.
- [10] P.P.A. Dhooge, D. Valkenburg, C.B. Hoyng, Gene therapy for inherited retinal diseases - ScienceDirect, *Gen. Genomics Eye Dis.* (2020) 279–295.
- [11] T.M. Buck, J. Wijnholds, Recombinant adeno-associated viral vectors (rAAV)-Vector Elements in ocular gene therapy clinical trials and transgene expression and bioactivity assays, *Int. J. Mol. Sci.* 21 (2020), <https://doi.org/10.3390/ijms21124197>.
- [12] M.F. Naso, B. Tomkowicz, W.L. Perry 3rd, W.R. Strohl, Adeno-associated virus (AAV) as a vector for gene therapy, *BioDrugs* 31 (2017) 317–334, <https://doi.org/10.1007/s40259-017-0234-5>.
- [13] W. Li, F. Kong, X. Li, X. Dai, X. Liu, Q. Zheng, R. Wu, X. Zhou, F. Lu, B. Chang, Q. Li, W.W. Hauswirth, J. Qu, J.J. Pang, Gene therapy following subretinal AAV5 vector delivery is not affected by a previous intravitreal AAV5 vector administration in the partner eye, *Mol. Vis.* 15 (2009) 267–275.
- [14] F. Kong, W. Li, X. Li, Q. Zheng, X. Dai, X. Zhou, S.L. Boye, W.W. Hauswirth, J. Qu, J.J. Pang, Self-complementary AAV5 vector facilitates quicker transgene expression in photoreceptor and retinal pigment epithelial cells of normal mouse, *Exp. Eye Res.* 90 (2010) 546–554, <https://doi.org/10.1016/j.exer.2010.01.011>.
- [15] J.J. Pang, A. Lauramore, W.T. Deng, Q. Li, T.J. Doyle, V. Chiodo, J. Li, W. W. Hauswirth, Comparative analysis of in vivo and in vitro AAV vector transduction in the neonatal mouse retina: effects of serotype and site of administration, *Vis. Res.* 48 (2008) 377–385, <https://doi.org/10.1016/j.visres.2007.08.009>.
- [16] D. Grimm, J.S. Lee, L. Wang, T. Desai, B. Akache, T.A. Storm, M.A. Kay, In vitro and in vivo gene therapy vector evolution via multispecies interbreeding and retargeting of adeno-associated viruses, *J. Virol.* 82 (2008) 5887–5911, <https://doi.org/10.1128/JVI.00254-08>.
- [17] Y. Katada, K. Kobayashi, K. Tsubota, T. Kurihara, Evaluation of AAV-DJ vector for retinal gene therapy, *PeerJ* 7 (2019) e6317, <https://doi.org/10.7717/peerj.6317>.
- [18] D. Sen, R.A. Gadkari, G. Sudha, N. Gabriel, Y.S. Kumar, R. Selot, R. Samuel, S. Rajalingam, V. Ramya, S.C. Nair, N. Srinivasan, A. Srivastava, G.R. Jayandharan, Targeted modifications in adeno-associated virus serotype 8 capsid improves its hepatic gene transfer efficiency in vivo, *Hum. Gene Ther. Methods* 24 (2013) 104–116, <https://doi.org/10.1089/hgtb.2012.195>.
- [19] L. Zhong, B. Li, G. Jayandharan, C.S. Mah, L. Govindasamy, M. Agbandje-McKenna, R.W. Herzog, K.A. Weigel-Van Aken, J.A. Hobbs, S. Zolotukhin, N. Muzyczka, A. Srivastava, Tyrosine-phosphorylation of AAV2 vectors and its consequences on viral intracellular trafficking and transgene expression, *Virology* 381 (2008) 194–202, <https://doi.org/10.1016/j.virol.2008.08.027>.
- [20] N. Gabriel, S. Hareendran, D. Sen, R.A. Gadkari, G. Sudha, R. Selot, M. Hussain, R. Dhaknamoorthy, R. Samuel, N. Srinivasan, A. Srivastava, G.R. Jayandharan, Bioengineering of AAV2 capsid at specific serine, threonine, or lysine residues improves its transduction efficiency in vitro and in vivo, *Hum. Gene Ther. Methods* 24 (2013) 80–93, <https://doi.org/10.1089/hgtb.2012.194>.
- [21] P. Pechan, H. Rubin, M. Lukason, J. Ardinger, E. DuFresne, W.W. Hauswirth, S. C. Wadsworth, A. Scaria, Novel anti-VEGF chimeric molecules delivered by AAV vectors for inhibition of retinal neovascularization, *Gene Ther.* 16 (2009) 10–16, <https://doi.org/10.1038/gt.2008.115>.
- [22] Y.M. Paulus, A. Sodhi, Anti-angiogenic therapy for retinal disease, *Handb. Exp. Pharmacol.* 242 (2017) 271–307, https://doi.org/10.1007/164_2016_78.
- [23] L.C. Byrne, B.E. Ozturk, T. Lee, C. Fortuny, M. Visel, D. Dalkara, D.V. Schaffer, J. G. Flannery, Retinoschisin gene therapy in photoreceptors, Muller glia or all retinal cells in the Rs1h^{-/-} mouse, *Gene Ther.* 21 (2014) 585–592, <https://doi.org/10.1038/gt.2014.31>.
- [24] C. Vijayasathary, Y. Zeng, M.J. Brooks, R.N. Fariss, P.A. Sieving, Genetic rescue of X-linked retinoschisis mouse (Rs1(-/y)) retina induces quiescence of the retinal microglial inflammatory state following AAV8-RS1 gene transfer and identifies gene networks underlying retinal recovery, *Hum. Gene Ther.* 32 (2021) 667–681, <https://doi.org/10.1089/hum.2020.213>.
- [25] G.J. Ye, T. Conlon, K. Erger, P. Sonnentag, A.K. Sharma, K. Howard, D.R. Knop, J. D. Chulay, Safety and biodistribution evaluation of rAAV2tYF-CB-hRS1, a recombinant adeno-associated virus vector expressing retinoschisin, in RS1-deficient mice, *Hum. Gene Ther. Clin. Dev.* 26 (2015) 177–184, <https://doi.org/10.1089/humc.2015.077>.
- [26] R.A. Bush, Y. Zeng, P. Colosi, S. Kjellstrom, S. Hiriyanna, C. Vijayasathary, M. Santos, J. Li, Z. Wu, P.A. Sieving, Preclinical dose-escalation study of intravitreal AAV-RS1 gene therapy in a mouse model of X-linked retinoschisis: dose-dependent expression and improved retinal structure and function, *Hum. Gene Ther.* 27 (2016) 376–389, <https://doi.org/10.1089/hum.2015.142>.
- [27] B.A. Scraggs, S. Bhattarai, M. Helms, I. Cherascu, A. Salesevic, E. Stalter, J. Laird, S.A. Baker, A.V. Drack, AAV2/4-RS1 gene therapy in the retinoschisin knockout mouse model of X-linked retinoschisis, *PLoS One* 17 (2022) e0276298, <https://doi.org/10.1371/journal.pone.0276298>.
- [28] S. Gorai, D. Paul, R. Borah, N. Haloi, M.K. Santra, D. Manna, Role of cationic groove and hydrophobic residues in phosphatidylinositol-dependent membrane-binding properties of tks5-phox homology domain, *ChemistrySelect* 3 (2018) 1205–1214, <https://doi.org/10.1002/slct.201702558>.